Review

Dynamic structural property of organic-inorganic metal halide perovskite

Jin-Wook Lee,[1,5] Seongrok Seo,[2,5] Pronoy Nandi,[2] Hyun Suk Jung,[3,*] Nam-Gyu Park,[4,*] and Hyunjung Shin[2,*]

Summary

Unique organic-inorganic hybrid semiconducting materials have made a remarkable breakthrough in new class of photovoltaics (PVs). Organic-inorganic metal (Pb and/or Sn) halides (-I, -Br, and -Cl) are the semiconducting absorber with the crystal structure of the famous "Perovskite". It is widely called "perovskite solar cells (PSCs)" in PV society. Now, the power conversion efficiency (PCE) of PSCs is recorded in 25.5%. Prototypical composition of the absorbers is (A = methylammonium [MA], formamidinium [FA], and Cs), (M = Pb and/or Sn), and (X = I, Br, and Cl) in the form of perovskite AMX_3. Since the report on the stable all solid-state PSCs in 2012, the average annual growth rate of PCE is well over $\sim$10%. Such an outstanding PV performance attracts huge number of scientists in our research society. Their chemical as well as physical properties are dramatically different from monocrystalline Si, GaAs, other III-IV semiconductors, and many oxides with the crystal structure of perovskite. In this review, different fundamental aspects, in particular, the dynamic properties of A site cationic molecules and PbI_6 octahedrons linked with their corners, from other semiconducting and dielectric materials are reviewed and summarized. Upon discussing unique properties, perspectives on the promising PV applications based on the comprehension in dynamic nature of the orientation in A site molecule and PbI_6 octahedron tilting will be given.

Introduction

Origin of high efficiencies exhibited by photovoltaics (PVs) and optoelectronic devices fundamentally based on organic-inorganic hybrid metal halides with the crystal structure of perovskite remains a subject of widespread research interest across the globe (Seo et al., 2019). The halide materials show great promise for decreasing the grid parity taking advantages of low-cost starting materials (Kim et al., 2012, 2020; Lee et al., 2019; Seo et al., 2019), high throughput (Brenner et al., 2016), and low-temperature fabrication techniques compared with the traditional monocrystalline Si and III-V PV devices (Brenner et al., 2016; Ding et al., 2020a; Kim et al., 2017; Lee et al., 2019; Seo et al., 2019). Not only the PV devices but also the superior optoelectronic properties of the halide perovskites enable application of the materials in a variety of devices including photodetectors (Chun et al., 2018; Saidaminov et al., 2015), light emitting diodes(Lee et al., 2017, 2020), transistors (Senanayak et al., 2017), memories (Kim et al., 2019; Yang et al., 2018), nanogenerators (Ding et al., 2020b), and spintronics (Wang et al., 2019).

Organic-inorganic hybrid lead halides, typically methylammonium (MA) and/or formamidinium (FA) lead triiodides, $MAPbI_3$, and $FAPbI_3$, are relatively new and unique class of materials. As a solar cell absorber, excellent optoelectronic properties were extensively researched and reported in the literature (Shi et al., 2015; Stranks et al., 2013; Xing et al., 2013; Yin et al., 2014). Traditionally, studies on the structure–property relationship in functional materials are often truly essential (Stoumpos and Kanatzidis, 2015; Zhou et al., 2020). Thus, it is important to understand the crystal structure of organic-inorganic hybrid perovskites, characterized by temperature-dependent crystal formation as well as phase transitions, considerable dynamic local disorder, various defects like lead cations, halogen anions and/or organic cations' vacancies or interstitials, to understand the underlying physics behind its high power conversion efficiencies (PCEs). The structure of organic-inorganic hybrid perovskite is, however, far more complicated than the

[1]SKKU Advanced Institute of Nanotechnology (SAINT) and Department of Nanoengineering, Sungkyunkwan University, Suwon 16419, Republic of Korea

[2]Department of Energy Science and Nature Inspired Materials Processing Research Center, Sungkyunkwan University, Suwon 16419, Republic of Korea

[3]School of Advanced Materials Science and Engineering, Sungkyunkwan University, Suwon 16419, Republic of Korea

[4]School of Chemical Engineering, Energy Frontier Laboratory, Sungkyunkwan University, Suwon 16419, Republic of Korea

[5]These authors contributed equally

*Correspondence:
hsjung1@skku.edu (H.S.J.),
npark@skku.edu (N.-G.P.),
hshin@skku.edu (H.S.)

https://doi.org/10.1016/j.isci.2020.101959

conventional inorganic solar cell absorbers like, Si, GaAs, CIGS, and, CdTe, etc., where an asymmetric and positively charged organic unit, i.e., MA and/or FA ion, with a permanent dipole, is surrounded by the corner-shared linkage of lead halide octahedron cages (Mashiyama et al., 1998; Poglitsch and Weber, 1987; Weber, 1978). Local vibrations of the linkage in corner-shared PbI_6 octahedral cages and vibration, orientation, and rotation of the A-site molecules make not possible to determine the decisive crystal structure. As a result, the understanding of semiconducting behaviors as absorbers obscured and thus optoelectronic performances.

Unique physical properties, for example, charge carrier generation and transport, of these perovskite materials need to be understood by focusing on the roles of (1) the motion of organic cations in screening and protecting carriers from trapping and recombination and (2) dynamic structural fluctuations, associated with ultrafast changes in local band structure and centrosymmetry, in facilitating charge separation and hindering recombination. Thus, we believe that careful review of structural investigations of hybrid organic-inorganic lead halide perovskites is essential for better understanding such a high performance in PV and optoelectronic devices. In addition, ferroelectricity could be also affected to the PV performances in perovskites. The ferroelectricity in hybrid metal halide perovskites has been originally ascribed to the collective rotational motion of monovalent organic molecular cations in A site, which might change the crystal structure of the perovskites from non-polar (I4/mcm) to polar (I4cm) tetragonal at room temperature (Frost et al., 2014; Quarti et al., 2014). Since then, many theoretical as well as experimental studies to reveal the ferroelectricity in the perovskites have been done, but still the presence of ferroelectricity in the perovskites at room temperature is not conclusive, yet. It is simply because that the dynamic rotational behavior of A-site molecules (MA as well as FA) affected to structurally instability with the PbI_6 octahedral cages. The ferroelectric properties in the perovskites may affect a lot to the PV performances, for example, abnormally large Voc, and less I-V hysteresis. And thus it is required to study the clear picture of both the A-site molecule motions and structural dynamics. (See, recent review paper by one of the authors (Nandi et al., 2020))

In this review, we summarized characteristic dynamic behaviors revealed from the perovskites in terms of tools for investigating it. The origin of the dynamic structure of the perovskites and possible optoelectronic properties associated it were first discussed, which was followed by introduction of precedented studies investigating the dynamic structure using various characterization tools. Finally, perspectives on the promising PV applications based on the comprehension in dynamic nature of the perovskite materials are presented.

General understanding of dynamic structural property

$MAPbI_3$, in particular, crystallizes in a perovskite crystal structure of AMX_3 type, where Pb and I atoms occupy M and X sites, respectively, and the inorganic cages consist of PbI_6 corner-sharing octahedra, which define a cuboctahedral cavity occupied by MA molecule as cation. Most of these perovskite materials crystallize in orthorhombic phase at even lower temperatures and have high/room temperature cubic phase depending on halide ions, with an intermediate tetragonal phase (Swsainson et al., 2003). At low temperature $MAPbI_3$ is in orthorhombic perovskite structure where MA ($CH_3NH_3^+$) dipoles ordering in an antiferroelectric arrangement, that is oriented in a head-to-tail fashion such to maximize the hydrogen bonding with the iodine atoms (Chi et al., 2005; Deretzis and La Magna, 2017; Mahale et al., 2016); however, the behavior of this dipole and their possible roles in determining the structural chemistry and material's properties in high temperature tetragonal and cubic phase is still developing (Baikie et al., 2013; Govinda et al., 2017). It is also suggested that the halogen ions exhibit disorder; i.e., PbX_6 octahedron is distorted in tetragonal/orthorhombic phases. In the tetragonal phase of $MAPbI_3$, stable at room temperature, the inorganic structure shows a characteristic octahedral tilting of the type $a^0a^0c^-$ (Bernasconi and Malavasi, 2017; Stoumpos et al., 2013; Wei et al., 2014), followed by the Glazer notation (Glazer, 1975). In other words, the tetragonal crystal structure resulted from PbX_6 octahedral tilting. In the halide perovskites, primary electronic band structures were determined by the octahedral network through the interaction between Pb and halides' orbitals, and thus, the octahedral tilting in the perovskites significantly affects the overlap between the atomic orbitals. Such a wide range of distortions, including polar distortions, has fueled the possibility of efficient charge separation and transfer in this type of materials (Beilsten-Edmands et al., 2015; Fan et al., 2015; Röhm et al., 2019). Alternate claims regarding the crystallographic structure of hybrid perovskite in tetragonal phase suggests it is in either polar (non-centrosymmetric) I4cm (Dang et al., 2015; Stoumpos et al., 2013) or centrosymmetric I4/mcm (Baikie et al., 2013; Poglitsch and Weber, 1987) space groups. Theoretical calculations demonstrated that the preferred stability of a set of polar structures over apolar ones, with an energy difference only within 0.1 eV and a conversion barrier in 0.2 eV per unit cell, thus
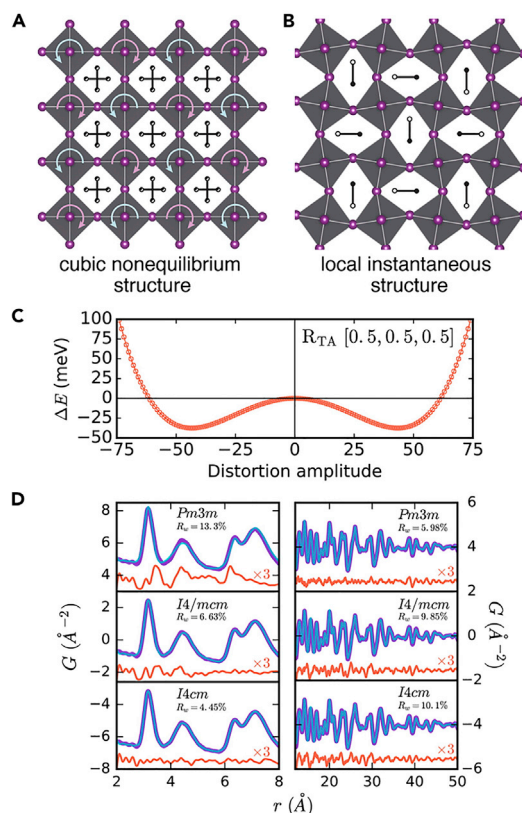
**Figure 1. Local symmetry breaking in MAPbI$_3$ at 350 K**

(A) Cubic nonequilibrium structure (free of distortions) and (B) Distortions from cubic symmetry generate anisotropic cavities and couple to motion of the MA cation, which was represented by off-centered and oriented along the long axis of the cavity.

(C) DFT-based lattice dynamic calculations show that the energy minimum at the R point at 350 K is displaced in a double-well potential that causes local symmetry breaking.

(D) Comparison of the experimental PDF (purple) to cubic (Pm$\bar{3}$m), centrosymmetric (I4/mcm), and noncentrosymmetric (I4cm) tetragonal models (blue) shows a superior fit for the low-symmetry models at low r (2–8 Å). However, the models perform oppositely at high r with the high-symmetry cubic structure giving the best agreement to the data in the 12–50 Å region. The residuals (orange) are scaled ×3 for clarity.

Credit Adapted from Beecher et al. (2016).

possibly accessible at room temperature. The I4cm and I4/mcm types of structure have markedly different in electronic band structures, despite showing a relatively small band gap variation (Quarti et al., 2014). Hence, careful high-resolution temperature dependent synchrotron X-ray diffraction measurements and/or Rietveld refinement are essential to understand the crystal structure of hybrid perovskites. High resolution synchrotron XRD revealed that preferred symmetry of hybrid perovskites is centrosymmetric rather than non-centrosymmetric. However, this description is often inconsistent with many different dynamic observations of MA ion dipoles such as: (i) totally free rotating of MA cation, (ii) rotating in a correlated manner, and (iii) not rotating, but freezes in an uncorrelated/random manner and results a glassy state. It is extremely difficult to probe the timescale of these dipoles accurately and identify the exact dynamic behavior of MA ions (Ren et al., 2016). Spatial anisotropy and selective ionic bonding of MA ions with the halide atoms of the inorganic cage influence the bond-length and bond-angle distributions, and consequently, the structural features of the crystal (Egger et al., 2018). It is also noted that molecular dipole orientations fluctuating on a picosecond timescale with the octahedral halide cages exhibit large anharmonic thermal fluctuations. The anharmonic effects are not limited to hybrid perovskites with molecular cations, but are also present in the all-inorganic, for example, CsPbBr$_3$, investigated by combining low-frequency Raman scattering with molecular dynamic simulations (Yaffe et al., 2017). Local symmetry breaking with a small cost of energy in MAPbI$_3$ at room temperature (R.T.) make the decisive determination of the crystal structure even characterized by the advanced techniques quite difficult (Figure 1) (Beecher et al., 2016) The
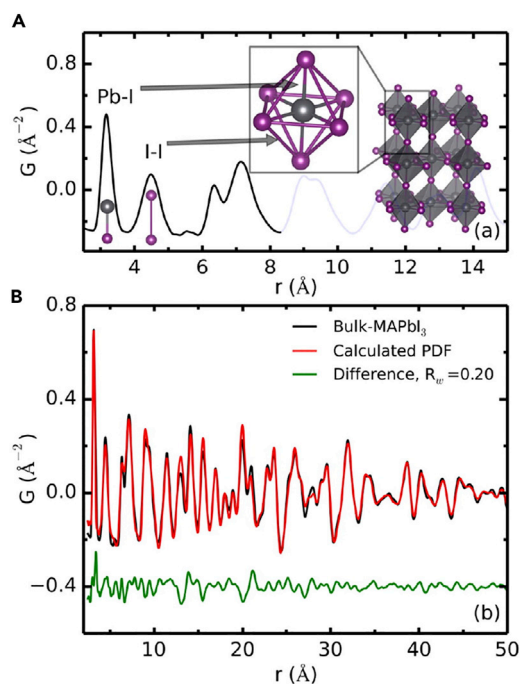
Figure 2. A PDF method providing atom to atom distances in bulk MAPbI$_3$

(A) A PDF of bulk MAPbI$_3$ perovskite. The first peak corresponds to the nearest neighbor distance (Pb–I), the second peak the shortest I–I distance, and so on.

(B) PDFs from bulk-MAPbI$_3$ (black) and the best-fit model (red) with the difference curve offset below (green). The experimental PDF from the highly crystalline reference perovskite sample shows a good match (Rw = 0.20) with the simulated PDF of the tetragonal structure (space group I4cm) (see inset in panel a and the main text for details).

Credit adapted from Choi et al. (2014).

large polar fluctuations may result in local dynamical movements of the electronic band gap, for instance, the conduction band splitting into lower indirect conduction energy bands, and thus play a key role in determining electronic properties of hybrid crystals (Motta et al., 2015; Quarti et al., 2016).

### Softness and anharmonicity characterized by X-ray and neutron scattering/diffraction

As stated earlier, one-unit cell has eight octahedral cages (MX$_6$) and the cation "A" is situated between each octahedra. Here the site, "A", represents the monovalent organic (MA or FA) or inorganic Cs$^+$ cation and "M" is mostly Pb^{2+}, while the anion, "X", is the halide ions (I$^-$, Br$^-$ or Cl$^-$) (Nandi et al., 2016). APbX$_3$ (X = I, Br, Cl) crystallizes in cubic perovskite structure at high temperature, satisfying Goldschmidt's tolerance factor, $t_G = (r_A + r_X)/\sqrt{2}(r_B + r_X) = 0.912$ (MAPbI$_3$), 0.927 (MAPbBr$_3$), 0.938 (MAPbCl$_3$), 0.987 (FAPbI$_3$), 1.008 (FAPbI$_3$), 1.023 (FAPbCl$_3$), 0.807 (CsPbI$_3$), 0.815 (CsPbBr$_3$), and 0.820 (CsPbCl$_3$) (Kim et al., 2020). It is noted that values of $t_G < 1$ result in octahedral tilting. Further, octahedral factor ($\mu = r_B/r_X$) are 0.541, 0.607, and 0.657 for APbI$_3$, APbBr$_3$, and APbCl$_3$, respectively (Kim et al., 2020).

Decisive structural determination of the phase of MAPbI$_3$ has been hindered by the inherent complexity with disorder in both organic and inorganic components. The inherent limitations of X-ray diffraction techniques; these include an inability to distinguish the near isoelectronic atoms, i.e., carbon and nitrogen, and difficulty in locating the light atom positions in the presence of the heavier atoms, Pb and I. The orientation of MA molecular cations and identification of hydrogen atomic position remained yet to be clarified. The atomic distortions in local structures and subtle compositional changes in MAPbI$_3$ were characterized by pair distribution function (PDF) analysis of X-ray total scattering data (Choi et al., 2014; Sanchez et al., 2019). This analysis revealed a presence of two nearly amorphous intermediate phases with local structures that share subtle but significant correlations with the PbI$_2$ precursor and the desired perovskite phase. Despite nearly identical crystal structure observed by powder X-ray diffraction, the local coordination environment reveals deviations in the octahedral lead-halide distances observed in PDF analysis of X-ray experimental data. A typical example for the tetragonal MAPbI$_3$ characterized by PDF is shown in Figure 2 (Choi et al., 2014). It is simply because of anharmonic lattice dynamics, which is modeled as rotational distortion of the PbX$_6$ octahedra. Tyson et al. also indicated a large degree of anharmonicity in the PbX$_6$ octahedra and speculate that the halide atoms can move considerably within the lattice at very low cost in energy (Tyson et al., 2017). It is also argued that the softness of the lattice which underlies the high anharmonicity, enable deformation of the lattice in response to the defect but limits its extension to a very small region of space yielding a material with resilient high carrier mobility in the presence of defects (Whitfield

et al., 2016; Zhu et al., 2016b). The atomic distortions due to off-center displacement of halogen atoms in local structures of MAPbI$_3$ were characterized by PDF analysis of X-ray total scattering data (Choi et al., 2014) and extended X-ray absorption fine structure measurement, which are powerful techniques to provide information on the local structure around a specific type of atoms (Sanchez et al., 2019; Worhatch et al., 2008). These local structure analyses showed that the PbX$_6$ octahedra is far from the undeformed model inferred from a traditional crystallographic description of Pm-$\bar{3}$m structure. Collectively, the results from the local structure indicate that the halogen atoms can move considerably within the lattice at very low cost in energy, which create a high density of defects each with limited spatial extension. This high flexibility of halides makes the system less structural stable than typical oxide perovskites, however, this halide flexibility maybe the reason of relatively high charge carrier mobility of hybrid perovskites.

Cubic perovskite structure contains only one formula unit (Z = 1); hence the non-centrosymmetric MA ion must be randomly oriented to satisfy O$_h$ symmetry. As the temperature is lowered, tetragonal and orthorhombic phases are stabilized with an accompanying ordering of MA$^+$ molecular ions (Wasylishen et al., 1985). Phase transition between cubic and tetragonal phases in MAPbI$_3$ was studied by temperature-dependent X-ray diffraction (XRD) in an interval between 30 and 100 °C. Using by normal XRD the phase transformation can be clearly observed. From the both phases of cubic and tetragonal of MAPbI$_3$ as drop- and spin-coated films several diffracting peaks are located at almost the same 2θ angle, even though the indexing differs. In higher symmetry, cubic phase, a few peaks disappeared, and some double peaks emerged into single peaks (Jacobsson et al., 2015). It has been studied the crystal structure in more detail by using a combined single crystal neutron/XRD and solid-state nuclear magnetic resonance (ss-NMR) (Baikie et al., 2015). They suggested hexagonal/rhombohedral cell with lattice constants of a = 8.9426(5) Å, b = 8.9428(6) Å, c = 10.9465(4) Å, alpha = 90.009(4), beta = 90.007(4), and gamma = 120.000(6) (the equivalent rhombohedral cell is a = 6.3222(4) Å and alpha = beta = gamma = 90.021(4)) for MAPbI$_3$, while only cubic symmetry was suggested for MAPbBr$_3$ and MAPbCl$_3$. Stoumpos et al., also indicated the high temperature 'cubic' phase to be metrically tetragonal with small differences in a and c lattice parameters (Stoumpos et al., 2013). A transformation from tetragonal to a rhombohedral cell would require a first-order phase transition. Previously calorimetry studies have shown that the high temperature phase transition for MAPbI$_3$ is of the first-order (but close to second order) (Onoda-Yamamuro et al., 1990). It is now clear that the MA units do not adopt fixed positions in the perovskite and are instead tumbling within the cages formed by PbI$_6$ octahedra in ambient and high temperature crystal structures. In the tetragonal modification, the MA molecule appears in eight different but symmetry-related positions because of the orientational disorder at each site. This orientational disorder of the MA molecule vanishes in the ordered orthorhombic (Pnma) low-temperature phase (Schuck et al., 2018). The geometrical arrangement of the MA group is not known in detail. At low temperature, the crystal adopts an orthorhombic (Pnma) structure, in which the PbI$_6$ octahedra are strongly deformed. Such deformation can restrict the rotational degrees of freedom of MA, thus imposing a spatial ordering to MAPbI$_3$, i.e., antiferroelectric. In this case the MA is pinned and can only rotate along the C-N axis. As the temperature is increased, the MA molecules become free to rotate between the octahedral cages. Above room temperature, such rotation is too fast to determine the exact location of MA groups. In any chance, the phase transition in perovskites could be driven by the organic component and not Pb-I network. Heat capacity along with temperature dependent XRD showed crystallographic phase transition from cubic (Pm-$\bar{3}$m) to tetragonal (I4/mcm) at a temperature of 330.8 K, 236.1 K, 177.2 K, 238 K and 403 K for MAPbI$_3$, MAPbBr$_3$, MAPbCl$_3$, and CsPbBr$_3$ (Hirotsu et al., 1974), respectively. It is quite unusual that during the phase transition clear anomalies were observed in heat capacity measurements in MAPbI$_3$ and/or MAPbBr$_3$ as indicated the first-order phase transition without breaking any major bonding in the structure instead of just tilting of PbI$_6$ octahedra and disorder of organic molecules, and thus the phase transition seems to be like the order-disorder type.

FAPbI$_3$-based perovskite's compositions are widely used for the fabrication of perovskite solar cells with the record high efficiency. The FAPbI$_3$-based compositions were reported to have superior charge carrier transporting properties, better thermal and light stability and a more ideal bandgap compared to the prototypical MAPbI$_3$-based ones. Comparing with the MAPbI$_3$, FAPbI$_3$ was relatively less studied. FA cation has relatively larger ionic radius of 253 pm than that of MA cation (217 pm), resulting in ~8.2% larger t$_G$ of 0.987. Such increase in t$_G$ causes metastability of high temperature cubic phase at room temperature, and relatively complex phase evolution depending on the temperature profiles.
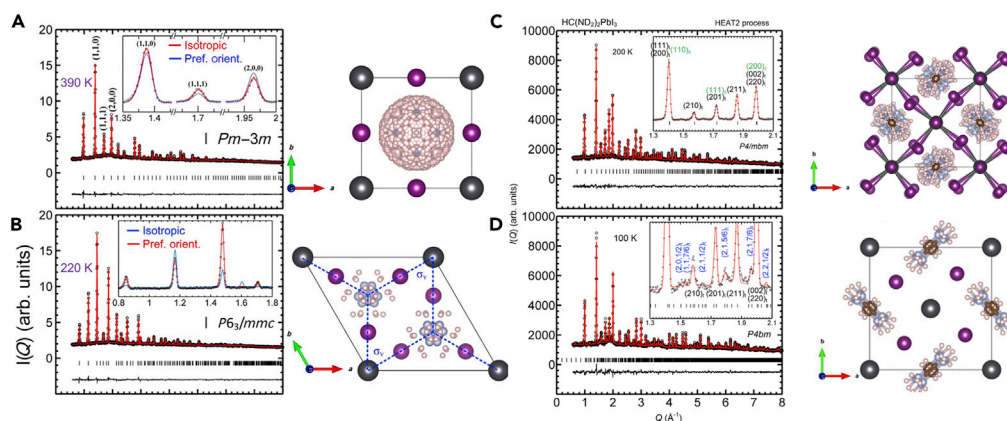
Figure 3. Neutron diffraction patterns of FAPbI₃

Measured at (A) 390 K, (B) 220 K for as synthesized powder. The data measured at (C) 200 K and (D) 100 K after *ex-situ* heating at 450 K for 30 min to induce the phase transition from hexagonal to cubic perovskite phase. Refined structures are on the right side of the measured data (A) cubic Pm3m (B) hexagonal P6₃/mmc (C) tetragonal P4bm and (D) tetragonal P4/mbm structure. The spheres in dark gray, violet, pink, and light blue represent Pb, I, H/D, and N atoms, respectively. Credit adapted from Chen et al. (2016).

Initially, high temperature perovskite phase of the FAPbI₃ was reported to be trigonal space groups with 3-fold disordered FA cation by XRD (Stoumpos et al., 2013). However, Weller et al. later reported that the high temperature phase adopts a cubic unit cell with a lattice constant of a = 6.3620(9) Å using a Neutron powder diffraction measurement (Weller et al., 2015). The trigonal planar FA cation was found to be in the central mirror plane of the unit cell with 12 disordered orientations with the fast re-orientational time constant of ~2 ps like the highly disordered MA cation in the cubic MAPbI₃. Chen et al. utilized the temperature dependent neutron diffraction measurement to investigate temperature dependent structural change of FAPbI₃ (Figure 3) (Chen et al., 2016). They confirmed a cubic structure of the high temperature FAPbI₃ phase with Pm$\bar{3}$m symmetry and lattice constant of a = 6.3855(2) Å. They suggested almost random orientation of FA cations (480 possible sites) in the cubic lattice at 390 K. The synthesized FAPbI₃ analyzed at 220 K, however, showed a hexagonal structured non-perovskite phase with P6₃/mmc space group and lattice constant of a = b = 8.6226(5) Å and c = 7.9458(5) Å where FA has 12 preferred orientations in the lattice. This indicates that the cubic perovskite phase of FAPbI₃ at room temperature is thermodynamically not favorable, which might be related with the relatively larger ionic radius of FA than that of MA. As formed hexagonal FAPbI₃ phase is transformed to cubic perovskite phase upon heating to ~400 K. Interestingly, the formed cubic phase remains stable upon cooling down to 8.2 K, which is far lower than the phase transition temperature. Based on the first-principle calculation, it was suggested that the freely rotating FA cation inside the cubic lattice has entropic contribution to the free energy of the cubic structure, which stabilize the cubic structure well below the hexagonal structure with energy barrier of ~0.6 eV for the reverse phase transition. Later, Chen et al. investigated band-edge carrier lifetimes in the low temperature FAPbI₃ perovskite phases (Chen et al., 2017). Using synchrotron XRD patterns, they found that the low temperature FAPbI₃ perovskite adopts P4bm and P4/mbm tetragonal structures at the temperature range of ~140 K < T < 280 K and < ~ 140 K, respectively. In the tetragonal phase, the organic molecules were found to have strong preferential orientations, indicating that change in the rotational dynamics of FA cation induces the temperature dependent phase transition. By correlating the phase transition behavior and photoluminescence (PL) lifetime, they also suggested that the rotational motion of the FA cation largely affect the band edge carrier lifetimes by inducing polaron effects to screen electrostatic interaction of the photo-excited charge carriers. As the temperature increases, isotropic rotational motion of the FA cation become active to induce phase transition from a tetragonal to cubic polymorph, and the charge carrier lifetime was significantly elongated with the screening effect of the freely rotating FA cation in the cubic lattice. This observation highlights important roles of dynamic organic cations not only in thermodynamic stability of the perovskite phase but also in charge carrier lifetimes in the crystals.

Rotational disorder of A-site molecules characterized by infrared spectroscopy

MA molecular cations occupied in A sites of perovskite AMX₃ crystal structure as stated earlier. Hydrogen bonding plays an important role in the interaction of the MA molecules and the inorganic metal halide octahedral building blocks. At room temperature, MA molecules can be occupied by eight different positions resulted
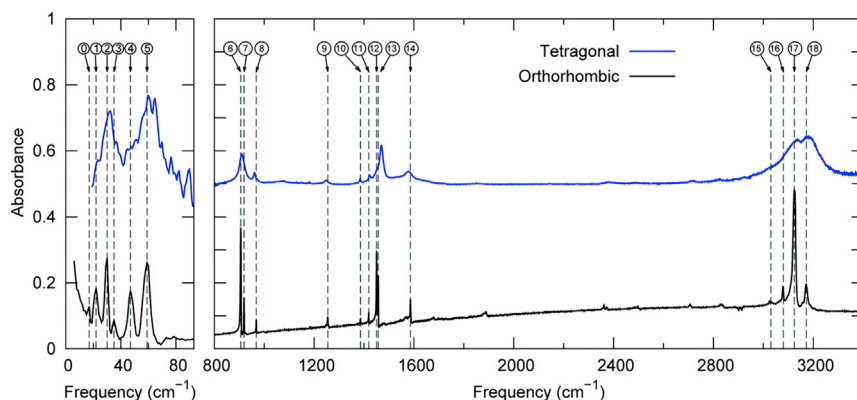
Figure 4. Comparison between the measured infrared spectra of the low-temperature orthorhombic phase (black curve) and the room temperature tetragonal phase (blue curve) of the MAPbI$_3$ perovskite

For clarity, the infrared spectrum of the tetragonal phase is offset vertically by 0.5 au. The spectra are measured at 10 and 295 K, respectively, at normal incidence. Differences in baseline are due to the fact that the room temperature data is reflection-corrected but the low temperature data is not. The vertical dashed lines are guides to the eye and are centered at the peaks of the orthorhombic phase. Credit adapted from Pérez-Osorio et al., 2015.

by orientational disorder at each site. While the organic cation does not directly participate in the formation of electronic transport levels, it influences the lattice constants and thereby indirectly the band gap. In particular, the orientational disorder is critical to determine crystal structure as in tetragonal phases and thus resulting electronic processes and transport. The disorderness of MA molecules was found to become even more significant for their excited states under illumination. It was also shown that the light-induced rotational disorder resulted hot-electron scattering and/or cooling characterized by time-resolved electron-scattering experiments (Wu et al., 2017). Earlier years before applying for PVs, the orientation and dynamics of the MA cations inside the inorganic structures has been already investigated (Chi et al., 2005; Knop et al., 1990; Poglitsch and Weber, 1987; Swainson et al., 2003; Wasylishen et al., 1985). Recent progress has also been made in understanding the interaction between MA molecules and lead halides cages by analyzing the fundamental frequencies of the MA molecules with infrared (IR) spectroscopic methods. Understanding the structural properties of the organic-inorganic metal halides, taking into consideration of their intrinsic dynamical disorder, is of critical importance to provide a complete picture for the highly efficient PVs.

Ab initio Car-Parrinello molecular dynamics simulations on the MAPbI$_3$ perovskites combined with the IR spectrum in the low frequency region, where the vibrational motions of the MA cations are expected, showed fast rotational motion of the organic cation inside the inorganic structure with rotational times of the order of 4–6 ps. The strong coupling of the dynamics of the organic ions and the inorganic counterpart results in a clear spectroscopic marker in the broad and not clearly defined band in between 200 and 300 cm^{-1} in the IR spectrum of MAPbI$_3$ (Mosconi et al., 2014). Glaser et al. also measured IR spectrum in the range of 700–3700 cm^{-1} at room temperature and assigned the IR peaks above 900 cm^{-1} to internal vibrations of MA (Glaser et al., 2015). More detailed analysis of the vibrational eigenmodes and frequencies calculated with density functional perturbation theory including a comprehensive factor group theory was reported. They calculated the intensities in the IR spectrum of MAPbI$_3$ compound at the low-temperature orthorhombic Pnma structure. According to their analysis, the IR spectrum consists of three regions, namely, the internal vibrations of the MA cations (800–3100 cm^{-1}), the vibration of the MA cations (140–180 cm^{-1}), and the internal vibrations of the PbI$_3$ network (<140 cm^{-1}) (Pérez-Osorio et al., 2015). Focusing on the interactions between the organic cations and the inorganic cage, complete vibrational study of MAPbI$_3$ including the infrared and non-resonant Raman spectra in the entire frequency range of 30–3400 cm^{-1} and in the temperature range 80–360 K was reported (Ivanovska et al., 2016; Leguy et al., 2016). See, the reported IR spectra of the low temperature orthorhombic phase and R.T. tetragonal phase of the MAPbI$_3$ in Figure 4 (Pérez-Osorio et al., 2015). Orientational dynamics of the organic cation in a range of pure- and mixed-halide perovskite materials is also reported (Selig et al., 2017).

Structural dynamics by ss-NMR

ss-NMR is a promising tool for characterization of dynamics for elements in a solid-state perovskite lattice. While diverse ss-NMR measurements enable a probe of the chemical environment and dynamics for
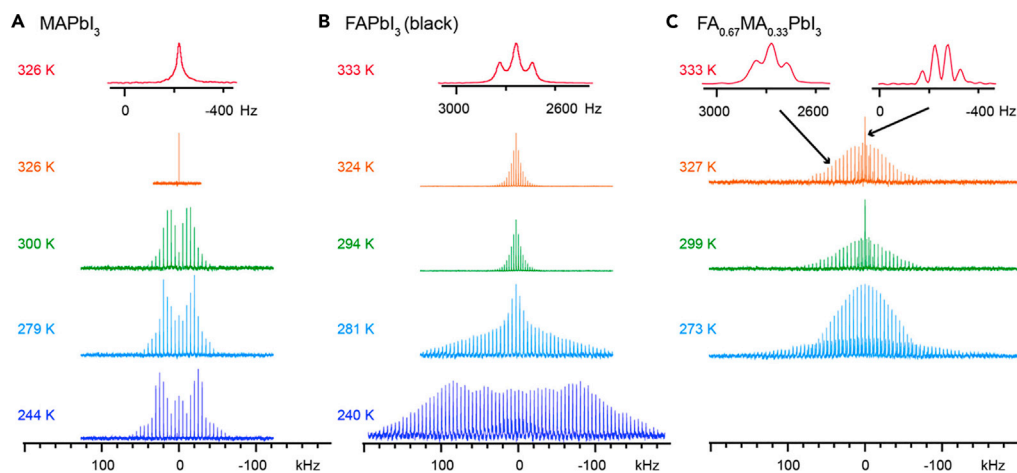
Figure 5. Solid-state ^{14}N echo-detected variable-temperature magic angle spinning (MAS) nuclear magnetic resonance (NMR) spectra of the perovskite powders with different compositions

(A–C) (A) $MAPbI_3$, (B) $FAPbI_3$, and (C) $FA_{0.67}MA_{0.33}PbI_3$. The MAS rate was either 3 or 5 kHz (between 240 and 327 K) and 20 kHz for the two top 333 K spectra in panels b and (C) The top insets (red) show a close-up of the central peak with a characteristic splitting due to the familiar J-coupling between the nitrogen and the proton.
Credit adapted from Kubicki et al., 2017a.

most of the nuclei present, it is particularly useful for characterization of the dynamics for A site organic cations in the hybrid perovskite. The combination of 2H and ^{14}N NMR spectroscopy was already used for investigating the thermally induced dynamic motion of the MA cation in $MAPbX_3$ (X = Cl, Br, I) in 1980s. In the study by Wasylishen et al. and Knop et al., temperature-dependent ^2H and ^{14}N NMR measurements were performed to extract the corresponding relaxation time (T_1) and to observe the splitting of resonance lines at the given temperature, enabling elucidation of cation reorientation properties of the $MAPbX_3$ perovskites (Knop et al., 1990; Wasylishen et al., 1985). The results indicate that the C-N bond in cubic $MAPbI_3$ phase at high temperature (cubic) reorientates in an isotopically at a rate comparable to that of freely rotating MA cation which becomes increasingly anisotropic (tetragonal) and then arrested in a lower temperature phase (orthorhombic). They correlated the reduction of the thermal motion of the cation on cooling with the observed structural change in lattice structure to induce the phase transition of the $MAPbX_3$ perovskites. Recently, several attempts have been made to utilize ss-NMR to study the local order and dynamics in the hybrid perovskite materials (Roiland et al., 2016; Rosales et al., 2016; Senocrate et al., 2017). For example, based on the change in chemical environment of the Pb ion upon interacting with different halide anions, stoichiometric uniformity of mixed halide perovskite (e.g. $MAPbX_{3-x}X_x$) was investigated using a ^{207}Pb solid-state NMR (Rosales et al., 2016). The ^{133}Cs, ^{87}Rb, ^{39}K, ^{13}C and ^{14}N ss-NMR spectra were effectively used to study the microscopic composition of the double-, triple-, and quadruple-cation containing perovskite compositions (Kubicki et al., 2017b). As the roles of the dynamic motion of the A site cation on charge carrier behaviors in perovskite has been studied, Kubicki et al. utilized the ssNMR for quantitative study of the cation reorientation dynamics and its relationship with the carrier lifetimes (Kubicki et al., 2017a). They used a stochastic Liouville formalism to simulate the experimental solid-state ^{14}N magic angle spinning (MAS) NMR spectra (Figure 5) and extracted the quantitative information on the rate of cation dynamics. The cation reorientation correlation time extracted from ^{14}N MAS NMR spectra were 108 $\pm$ 18 ps for $MAPbI_3$ at 300 K and 8.7 $\pm$ 0.5 ps for $FAPbI_3$ at 294 K. It was noted that the FA cation rotates faster than MA cations in the cubo-octahedral cage regardless of its bulkier size. It is correlated with the longer charge carrier lifetime in $FAPbI_3$ than that in $MAPbI_3$ and the previous works that attributed the longer charge carrier lifetimes of the hybrid perovskites to a large polaron effect by interaction of charge carriers and dynamic cations (Miyata et al., 2017a, 2017b; Zhu et al., 2016a). For example, Chen et al. studied the composition and temperature dependent PL lifetime of the perovskite crystals and found that (1) $FAPbI_3$ shows longer PL lifetime (~260 ns) than $MAPbI_3$ (~11 ns) when they are in both cubic phase, (2) in both $MAPbI_3$ and $FAPbI_3$, PL lifetime dramatically increases as they converted from tetragonal to cubic phase as temperature rises (Chen et al., 2017). Such composition and temperature-dependent PL lifetime can be both correlated with change in rotational mode of the organic cation in the lattice and thus the polaron effect. We noted

that IR spectroscopy has been mostly used for studying dynamic motion of the organic cation in simple compositions (e.g. $MAPbI_3$) and that of lead halide lattice. On the other hand, the ss-NMR was used for characterizing the dynamic motion of the organic cation in the various compositions including mixed-cation perovskites (e.g. $FA_{1-x}MA_xPbI_3$) and their local order. In terms of studying the dynamic structure, one primary advantage of the ss-NMR over other characterization tools might be that it can study the dynamic motion of the individual cations in the mixed cation compositions by decoupling the spectra originated from each cation (Figure 5). For example, the cation reorientation correlation times in $FA_{0.67}$-$MA_{0.33}PbI_3$ perovskite were acquired as 133 ± 46 ps for MA and 12 ± 5 ps for FA ; the cations in the mixed phase rotate at the same rate as they were in the respective pure phase. They also applied the same approach to study the dynamics of guanidinium (GA) cation in the mixed cation perovskites ($GA_xMA_{1-x}PbI_3$) (Kubicki et al., 2018). The observed cation reorientation rate for the GA cation in $GA_{0.25}$-$MA_{0.75}PbI_3$ was in the rage of $<18 \pm 8$ ps, which is faster than that of MA in the same composition. Faster reorientation rate of the GA cation was correlated with the longer charge carrier lifetime in the $GA_{0.25}$-$MA_{0.75}PbI_3$ (369 ± 4 ns) than that in pure $MAPbI_3$ (81 ± 2 ns) perovskite, resulting in enhanced PV performance of the device with the GA incorporation. Because of the Pb-X octahedral networks directly affecting optoelectronic properties of the perovskite materials, engineering of the A site cation becomes one of the promising approaches to tune physico-chemical and optoelectronic properties of the perovskite film, and thus performance and stability of the devices (Alanazi et al., 2019; Lee et al., 2018; Tan et al., 2020). Accordingly, the solid-state NMR may become an important characterization tool to investigate not only the local ordering of the crystals but also the dynamics of the organic A site cations in the crystal lattice to find the perovskite compositions with better performance and stability.

Possible imaging of structural dynamics in transmission electron microscopy

Although the significance of elucidating the unique properties of halide perovskite is via analytical methods, the understanding of the structure-property relationship of halide perovskite is still underdeveloped. For example, it has not been fully understood how organic A-cations were arranged in halide perovskites crystal, whether they were localized or delocalized (Egger et al., 2018). Local vibrations of $[PbX_6]^{4-}$ octahedral cage in halide perovskite are also unclear, which leads to the possibility of changes in properties and crystal symmetry (Miyata et al., 2017a). This is different from the successful structure-property analysis by transmission electron microscopy (TEM) in the case of oxide perovskites and other inorganic semiconductors (Jia et al., 2003), relatively 'softer' halide perovskite undergo severe damage during electron beam irradiation, which makes the precise analysis much more challenging (Bekenstein et al., 2015). Several reliable examples of TEM observations of halide perovskites were reported by reducing the amount of accumulated electron dose to the specimen. We will briefly introduce these recent progresses coupled with important issues of halide perovskite.

The most studied proto-typical material, $MAPbI_3$, shows obvious electron beam sensitive nature during TEM experiments, which leaves structural analysis elusive. Initial literatures on electron diffraction or FFT (fast-Fourier transform) patterns of $MAPbI_3$ results did not exactly match the tetragonal phase that is original room temperature phase of $MAPbI_3$. Diffraction spots, typically observed in X-ray diffraction, are absent in TEM observation along the [001] zone axis direction in many reports (Kollek et al., 2015; Long et al., 2017; Son et al., 2016; Zhu et al., 2015). Kim et al. proposed the missing are due to the difficulty of the detecting the spots under the low electron beam intensity (Kim et al., 2018). It is also addressed that a high energy electron beam can induce side effects in halide perovskite such as the defect formation and intermediate phases by electron irradiation (Xiao et al., 2015). In TEM measurement, the electron dose rate can commonly reached to 104–105 e $Å^{-2}$ s^{-1} in high resolution (magnification) condition, which is enough to cause degradation in several phases (Dang et al., 2017). The reducing electron dose has been considered to be the minimum requirement for the precise observation of halide perovskite TEM specimen. Kim et al. addressed the coexistence of cubic and tetragonal phases in $MAPbI_3$ was identified by TEM measurement with low electron dose condition while non-perfect tetragonal diffraction spots were obtained. The distinguished two phases are revealed by the line profile of electron diffraction intensity. Rothmann et al. have investigated the structural and compositional change of $MAPbI_3$ during TEM observation by varying the amount of electron dose (Rothmann et al., 2018). They found some original diffraction spots of $MAPbI_3$ were blurred and forbidden spots were displayed over the time evolution even under the low electron dose rate of ~ 2 e $Å^{-2}$ s^{-1}. It was also confirmed that the lattice constant decreased over the time elapsed while the iodine to lead ratios decreased simultaneously. They argued that diffraction patterns of $MAPbI_3$ claimed in many publications more closely
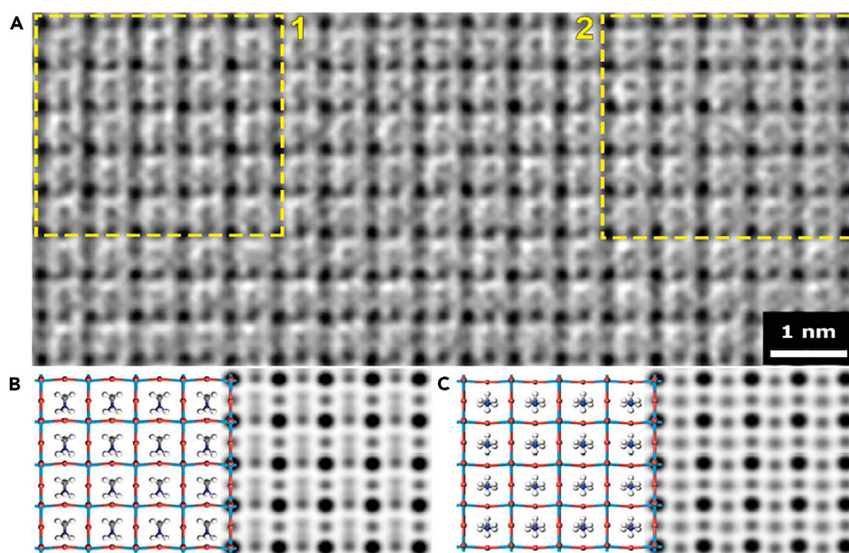
Figure 6. HRTEM of organic-inorganic hybrid perovskite MAPbBr$_3$

(A) CTF-corrected denoised HRTEM image. The squares highlight two ordered domains with off-centered MA cations that have differing orientations.

(B and C) The structural model (left) and the simulated projected potential map (right) of MAPbBr$_3$ with different MA orientations, corresponding to region 1 and 2 in (A), respectively. In (B) and (C), the off-centered MA cations exhibit normal and parallel configurations (relative to the projection direction), giving rise to in-plane and out-of-plane electric dipoles, respectively.

Credit adapted from Zhang et al. (2018).

matches the patterns when the degradations happen. The pristine diffraction pattern of MAPbI$_3$ corresponding to the tetragonal phase could be obtained by reducing the total amount of dose accumulated. Although the accurate and pristine diffraction patterns of tetragonal MAPbI$_3$ were successfully obtained, there is still a lack of understanding of fine structure such as local vibration and MA cation dynamics which can be observed by high resolution TEM imaging.

The atomic resolution images of halide perovskite have been reported by several groups with more stable MAPbBr$_3$ or inorganic CsPbBr$_3$ materials. To reduce electron dose rate, Yu et al. have succeeded in imaging the pristine structure of 2-dimensional CsPbBr$_3$ ultrathin (2–3 monolayers, MLs) nanosheet in atomic resolution using low does-rate in line holography (Yu et al., 2016). This technique achieves high signal to noise by reconstructing the electron exit-wave function. They confirmed that co-existing phase (cubic and orthorhombic) is present in a pristine structure in 2-dimensional CsPbBr$_3$ nanosheet at a dose rate of ~100 e Å^{-2} s^{-1} using in line holography method. A region is assigned to cubic phase and another region is orthorhombic, where distinct two phases are locally distributed, and the difference between two regions is further revealed through the FFT, which is corresponding to simulated results. This is the first reliable atomic resolution image observed *via* TEM under low electron dose conditions, and interestingly demonstrated that both phases can be co-existing in the halide perovskite. In the subsequent study, they obtained atomic resolution images of little thicker CsPbBr$_3$ of ~11 MLs by applying in line holography AC-STEM (Yu et al., 2017). They found 2-dimensional crystal structure of Ruddlesden-Popper phases coexist with cubic and orthorhombic phases in a single nanosheet. However, it cannot be ruled out the possibility of damage to the sample by high electron dose (50 pA electron probe). Zhang et al. has developed a one-step alignment of the zone axis method to observe atomic resolution images of electron beam sensitive materials with a low dose rate (3.7 e Å^{-2} s^{-1} for MAPbBr$_3$) (Zhang et al., 2018). They found MAPbBr$_3$ nanocrystals of 1–2 nm sized domains having locally distinct orientations of MA cation molecules (in-plane and out-of-plane direction of electrical dipoles relative to the projection, respectively) as shown in Figure 6 (Zhang et al., 2018). It is expected to be useful for understanding the ferroelectric characteristics derived from the structure-property relation by observing the movement and arrangement of MA cation molecules at the atomic scale. TEM is a powerful characterization tools to understand the structure-property relationship in halide perovskites that is not fully understood. It is still remained to be explored that how organic

cations are arranged inside the crystal structures and is it really having distinct local phase difference in these materials, which some results agree while others not. The unique properties of halide perovskite can be elucidated by further TEM-related research through answering some of interesting issues.

Summary and perspectives

The characteristic dynamic structure of the halide perovskites was suggested to be one of the origins of the superior optoelectronic properties such as long charge carrier lifetimes. As a result, noticeable efforts to elucidate the dynamic structure of the perovskite materials have been made based on a variety of characterization tools such as X-ray scattering/diffraction, IR spectroscopy, solid-state NMR measurement, and advanced TEM. Analyses of X-ray scattering/diffraction assist in identification of local structure indicating considerably mobile halogen atoms with relatively low activation energy, creating a high density of defects each with limited spatial extension. While the commonly used X-ray scattering/diffraction has some limitation on characterization of light and resonant organic cations, the IR and NMR spectroscopy effectively unraveled the dynamic motion of the A site cation, which was correlated with charge carrier lifetimes as well as the temperature dependent phase transition behavior of the halide perovskites. Nevertheless, fundamental understanding on the dynamic structure still remain as a challenge because of the 'soft' and thus vulnerable nature of the perovskite materials. In particular, observation of atomic scale microstructure by a TEM measurement was found to be extremely challenging due to severe degradation of the lattice structure under electron beam irradiation. Although reliable TEM images of the compositions with a relatively higher stability were acquired based on low dose measurements, characterization of the commonly used compositions are still missing.

While the material engineering of the perovskites has been relied on conventional 'static' crystal structure of the perovskite materials so far, understanding on the dynamic structure seems to be a prerequisite for design of advanced perovskite compositions with more reliable design rules. For example, precise elucidation of dynamic landscapes for A site cations and their interaction with photo-excited charge carriers would facilitate design of optimum A site cation for the longer charge carrier lifetimes. Investigation of various systems with many different A site cations not only under the ambient condition but also under realistic operational conditions with photo-excited charge carriers might be helpful to construct the design rules. Furthermore, dynamics of halide ions and their degree of freedom might be important not only for carrier lifetimes but also for operational stability of the devices. Although many strategies have been devised to suppress or mitigate ion migration in the perovskite materials detrimental to operational stability of the devices, design of new compositions of high energy barrier for ion migration would be fundamental solution toward the operational stability, which requires an accurate blueprint on local structure surrounding the halide ions. Finally, construction of atomic resolution images of pristine perovskite lattices as well as the different kinds of defects at bulk and grain boundaries will enable cogitation of effective strategies toward structural and defect engineering of perovskite materials.

Author contributions

J.-W. L. and S.S. contributed equally to this work.

References

Alanazi, A.Q., Kubicki, D.J., Prochowicz, D., Alharbi, E.A., Bouduban, M.E., Jahanbakhshi, F., Mladenović, M., Milić, J.V., Giordano, F., and Ren, D. (2019). Atomic-level microstructure of efficient formamidinium-based perovskite solar cells stabilized by 5-ammonium valeric acid iodide revealed by multinuclear and two-dimensional solid-state NMR. J. Am. Chem. Soc. 141, 17659–17669.

Baikie, T., Barrow, N.S., Fang, Y., Keenan, P.J., Slater, P.R., Piltz, R.O., Gutmann, M., Mhaisalkar, S.G., and White, T.J. (2015). A combined single crystal neutron/X-ray diffraction and solid-state nuclear magnetic resonance study of the hybrid perovskites $CH_3NH_3PbX_3$ (X = I, Br and Cl). J. Mater. Chem. A 3, 9298–9307.

Baikie, T., Fang, Y., Kadro, J.M., Schreyer, M., Wei, F., Mhaisalkar, S.G., Graetzel, M., and White, T.J. (2013). Synthesis and crystal chemistry of the hybrid perovskite $(CH_3NH_3)PbI_3$ for solid-state

sensitised solar cell applications. J. Mater. Chem. A 1, 5628–5641.

Beecher, A.N., Semonin, O.E., Skelton, J.M., Frost, J.M., Terban, M.W., Zhai, H., Alatas, A., Owen, J.S., Walsh, A., and Billinge, S.J.L. (2016). Direct observation of dynamic symmetry breaking above room temperature in methylammonium lead iodide perovskite. ACS Energy Lett. 1, 880–887.

Beilsten-Edmands, J., Eperon, G., Johnson, R., Snaith, H., and Radaelli, P. (2015). Non-ferroelectric nature of the conductance hysteresis in CH$_3$NH$_3$PbI$_3$ perovskite-based photovoltaic devices. Appl. Phys. Lett. 106, 173502.

Bekenstein, Y., Koscher, B.A., Eaton, S.W., Yang, P., and Alivisatos, A.P. (2015). Highly luminescent colloidal nanoplates of perovskite cesium lead halide and their oriented assemblies. J. Am. Chem. Soc. 137, 16008–16011.

Bernasconi, A., and Malavasi, L. (2017). Direct evidence of permanent octahedra distortion in MAPbBr$_3$ hybrid perovskite. ACS Energy Lett. 2, 863–868.

Brenner, T.M., Egger, D.A., Kronik, L., Hodes, G., and Cahen, D. (2016). Hybrid organic—inorganic perovskites: low-cost semiconductors with intriguing charge-transport properties. Nat. Rev. Mater. 1, 1–16.

Chen, T., Chen, W.-L., Foley, B.J., Lee, J., Ruff, J.P.C., Ko, J.Y.P., Brown, C.M., Harriger, L.W., Zhang, D., Park, C., et al. (2017). Origin of long lifetime of band-edge charge carriers in organic–inorganic lead iodide perovskites. Proc. Natl. Acad. Sci. U S A 114, 7519–7524.

Chen, T., Foley, B.J., Park, C., Brown, C.M., Harriger, L.W., Lee, J., Ruff, J., Yoon, M., Choi, J.J., and Lee, S.-H. (2016). Entropy-driven structural transition and kinetic trapping in formamidinium lead iodide perovskite. Sci. Adv. 2, e1601650.

Chi, L., Swainson, I., Cranswick, L., Her, J.-H., Stephens, P., and Knop, O. (2005). The ordered phase of methylammonium lead chloride CH$_3$ND$_3$PbCl$_3$. J. Solid State Chem. 178, 1376–1385.

Choi, J.J., Yang, X., Norman, Z.M., Billinge, S.J.L., and Owen, J.S. (2014). Structure of methylammonium lead iodide within mesoporous titanium dioxide: active material in high-performance perovskite solar cells. Nano Lett. 14, 127–133.

Chun, D.H., Choi, Y.J., In, Y., Nam, J.K., Choi, Y.J., Yun, S., Kim, W., Choi, D., Kim, D., and Shin, H. (2018). Halide perovskite nanopillar photodetector. ACS nano 12, 8564–8571.

Dang, Y., Liu, Y., Sun, Y., Yuan, D., Liu, X., Lu, W., Liu, G., Xia, H., and Tao, X. (2015). Bulk crystal growth of hybrid perovskite material CH$_3$NH$_3$PbI$_3$. CrystEngComm 17, 665–670.

Dang, Z., Shamsi, J., Akkerman, Q.A., Imran, M., Bertoni, G., Brescia, R., and Manna, L. (2017). Low-temperature electron beam-induced transformations of cesium lead halide perovskite nanocrystals. ACS Omega 2, 5660–5665.

Deretzis, I., and La Magna, A. (2017). Exploring the orthorhombic–tetragonal phase transition in

CH$_3$NH$_3$PbI$_3$: the role of atom kinetics. Nanoscale 9, 5896–5903.

Ding, R., Liu, C.-K., Wu, Z., Guo, F., Pang, S.-Y., Wong, L.W., Io, W.F., Yuan, S., Wong, M.-C., and Jedrzejczyk, M.B. (2020a). A general wet transferring approach for diffusion-facilitated space-confined grown perovskite single-crystalline optoelectronic thin films. Nano Lett. 20, 2747–2755.

Ding, R., Wong, M.-C., and Hao, J. (2020b). Recent advances in hybrid perovskite nanogenerators. EcoMat 2, e12057.

Egger, D.A., Bera, A., Cahen, D., Hodes, G., Kirchartz, T., Kronik, L., Lovrincic, R., Rappe, A.M., Reichman, D.R., and Yaffe, O. (2018). What remains unexplained about the properties of halide perovskites? Adv. Mater. 30, 1800691.

Fan, Z., Xiao, J., Sun, K., Chen, L., Hu, Y., Ouyang, J., Ong, K.P., Zeng, K., and Wang, J. (2015). Ferroelectricity of CH$_3$NH$_3$PbI$_3$ perovskite. J. Phys. Chem. Lett. 6, 1155–1161.

Frost, J.M., Butler, K.T., Brivio, F., Hendon, C.H., van Schilfgaarde, M., and Walsh, A. (2014). Atomistic origins of high-performance in hybrid halide perovskite solar cells. Nano Lett. 14, 2584–2590.

Glaser, T., Müller, C., Sendner, M., Krekeler, C., Semonin, O.E., Hull, T.D., Yaffe, O., Owen, J.S., Kowalsky, W., Pucci, A., et al. (2015). Infrared spectroscopic study of vibrational modes in methylammonium lead halide perovskites. J. Phys. Chem. Lett. 6, 2913–2918.

Glazer, A. (1975). Simple ways of determining perovskite structures. Acta crystallographica section A: crystal physics, diffraction. Theor. Gen. Crystallogr. 31, 756–762.

Govinda, S., Kore, B.P., Bokdam, M., Mahale, P., Kumar, A., Pal, S., Bhattacharyya, B., Lahnsteiner, J., Kresse, G., and Franchini, C. (2017). Behavior of methylammonium dipoles in MAPbX$_3$ (X= Br and I). J. Phys. Chem. Lett. 8, 4113–4121.

Hirotsu, S., Harada, J., Iizumi, M., and Gesi, K. (1974). Structural phase transitions in CsPbBr$_3$. J. Phys. Soc. Jpn. 37, 1393–1398.

Ivanovska, T., Quarti, C., Grancini, G., Petrozza, A., De Angelis, F., Milani, A., and Ruani, G. (2016). Vibrational response of methylammonium lead iodide: from cation dynamics to phonon–phonon interactions. ChemSusChem 9, 2994–3004.

Jacobsson, T.J., Schwan, L.J., Ottosson, M., Hagfeldt, A., and Edvinsson, T. (2015). Determination of thermal expansion coefficients and locating the temperature-induced phase transition in methylammonium lead perovskites using X-ray diffraction. Inorg. Chem. 54, 10678–10685.

Jia, C.L., Lentzen, M., and Urban, K. (2003). Atomic-resolution imaging of oxygen in perovskite ceramics. Science 299, 870–873.

Kim, H.-S., Lee, C.-R., Im, J.-H., Lee, K.-B., Moehl, T., Marchioro, A., Moon, S.-J., Humphry-Baker, R., Yum, J.-H., Moser, J.E., et al. (2012). Lead iodide perovskite sensitized all-solid-state submicron thin film mesoscopic solar cell with efficiency exceeding 9%. Sci. Rep. 2, 591.

Kim, J.Y., Lee, J.-W., Jung, H.S., Shin, H., and Park, N.-G. (2020). High-efficiency perovskite solar cells. Chem. Rev. 120, 7867–7918.

Kim, T.W., Uchida, S., Matsushita, T., Cojocaru, L., Jono, R., Kimura, K., Matsubara, D., Shirai, M., Ito, K., Matsumoto, H., et al. (2018). Self-organized superlattice and phase coexistence inside thin film organometal halide perovskite. Adv. Mater 30, 1705230.

Kim, Y., Bae, C., Jung, H.S., and Shin, H. (2019). Enhanced stability of guanidinium-based organic-inorganic hybrid lead triiodides in resistance switching. APL Mater. 7, 081107.

Kim, Y.C., Kim, K.H., Son, D.-Y., Jeong, D.-N., Seo, J.-Y., Choi, Y.S., Han, I.T., Lee, S.Y., and Park, N.-G. (2017). Printable organometallic perovskite enables large-area, low-dose X-ray imaging. Nature 550, 87–91.

Knop, O., Wasylishen, R.E., White, M.A., Cameron, T.S., and Oort, M.J.V. (1990). Alkylammonium lead halides. Part 2. CH$_3$NH$_3$PbX$_3$ (X= Cl, Br, I) perovskites: cuboctahedral halide cages with isotropic cation reorientation. Can. J. Chem. 68, 412–422.

Kollek, T., Gruber, D., Gehring, J., Zimmermann, E., Schmidt-Mende, L., and Polarz, S. (2015). Porous and shape-anisotropic single crystals of the semiconductor perovskite CH$_3$NH$_3$PbI$_3$ from a single-source precursor. Angew. Chem. Int. Ed. 54, 1341–1346.

Kubicki, D.J., Prochowicz, D., Hofstetter, A., Péchy, P., Zakeeruddin, S.M., Grätzel, M., and Emsley, L. (2017a). Cation dynamics in mixed-cation (MA)$_x$(FA)$_{1-x}$PbI$_3$ hybrid perovskites from solid-state NMR. J. Am. Chem. Soc. 139, 10055–10061.

Kubicki, D.J., Prochowicz, D., Hofstetter, A., Zakeeruddin, S.M., Grätzel, M., and Emsley, L. (2017b). Phase segregation in Cs-, Rb-and K-doped mixed-cation (MA)$_x$(FA)$_{1-x}$PbI$_3$ hybrid perovskites from solid-state NMR. J. Am. Chem. Soc. 139, 14173–14180.

Kubicki, D.J., Prochowicz, D., Hofstetter, A., Saski, M., Yadav, P., Bi, D., Pellet, N., Lewiński, J., Zakeeruddin, S.M., and Grätzel, M. (2018). Formation of Stable mixed guanidinium–methylammonium phases with exceptionally long carrier lifetimes for high-efficiency lead iodide-based perovskite photovoltaics. J. Am. Chem. Soc. 140, 3345–3351.

Lee, D.-K., Jeong, D.-N., Ahn, T.K., and Park, N.-G. (2019). Precursor engineering for a large-area perovskite solar cell with> 19% efficiency. ACS Energy Lett. 4, 2393–2401.

Lee, J.-W., Choi, Y.J., Yang, J.-M., Ham, S., Jeon, S.K., Lee, J.Y., Song, Y.-H., Ji, E.K., Yoon, D.-H., Seo, S., et al. (2017). In-situ formed type I nanocrystalline perovskite film for highly efficient light-emitting diode. ACS Nano 11, 3311–3319.

Lee, J.-W., Dai, Z., Han, T.-H., Choi, C., Chang, S.-Y., Lee, S.-J., De Marco, N., Zhao, H., Sun, P., Huang, Y., et al. (2018). 2D perovskite stabilized phase-pure formamidinium perovskite solar cells. Nat. Commun. 9, 3021.

Lee, J.-W., Tan, S., Han, T.-H., Wang, R., Zhang, L., Park, C., Yoon, M., Choi, C., Xu, M., Liao, M.E., et al. (2020). Solid-phase hetero epitaxial growth

of α-phase formamidinium perovskite. Nat. Commun. 11, 5514.

Leguy, A.M.A., Goñi, A.R., Frost, J.M., Skelton, J., Brivio, F., Rodríguez-Martínez, X., Weber, O.J., Pallipurath, A., Alonso, M.I., Campoy-Quiles, M., et al. (2016). Dynamic disorder, phonon lifetimes, and the assignment of modes to the vibrational spectra of methylammonium lead halide perovskites. Phys. Chem. Chem. Phys. 18, 27051–27066.

Long, M., Zhang, T., Zhu, H., Li, G., Wang, F., Guo, W., Chai, Y., Chen, W., Li, Q., Wong, K.S., et al. (2017). Textured $CH_3NH_3PbI_3$ thin film with enhanced stability for high performance perovskite solar cells. Nano Energy 33, 485–496.

Mahale, P., Kore, B., Mukherjee, S., Pavan, M., De, C., Ghara, S., Sundaresan, A., Pandey, A., Guru, T.R., and Sarma, D. (2016). Is $CH_3NH_3PbI_3$ polar? J. Phys. Chem. Lett. 7, 2412–2419.

Mashiyama, H., Kurihara, Y., and Azetsu, T. (1998). Disordered cubic perovskite structure of $CH_3NH_3PbX_3$ (X= Cl, Br, I). J. Korean Phys. Soc. 32, S156–S158.

Miyata, K., Atallah, T.L., and Zhu, X.-Y. (2017a). Lead halide perovskites: crystal-liquid duality, phonon glass electron crystals, and large polaron formation. Sci. Adv. 3, e1701469.

Miyata, K., Meggiolaro, D., Trinh, M.T., Joshi, P.P., Mosconi, E., Jones, S.C., De Angelis, F., and Zhu, X.-Y. (2017b). Large polarons in lead halide perovskites. Sci. Adv. 3, e1701217.

Mosconi, E., Quarti, C., Ivanovska, T., Ruani, G., and De Angelis, F. (2014). Structural and electronic properties of organo-halide lead perovskites: a combined IR-spectroscopy and ab initio molecular dynamics investigation. Phys. Chem. Chem. Phys. 16, 16137–16144.

Motta, C., El-Mellouhi, F., Kais, S., Tabet, N., Alharbi, F., and Sanvito, S. (2015). Revealing the role of organic cations in hybrid halide perovskite $CH_3NH_3PbI_3$. Nat. Commun. 6, 7026.

Nandi, P., Giri, C., Joseph, B., Rath, S., Manju, U., and Topwal, D. (2016). $CH_3NH_3PbI_3$, A potential solar cell candidate: structural and spectroscopic investigations. J. Phys. Chem. A 120, 9732–9739.

Nandi, P., Topwal, D., Park, N.-G., and Shin, H. (2020). Organic-inorganic hybrid lead halides as absorbers in perovskite solar cells: a debate on ferroelectricity. J. Phys. D Appl. Phys. 53, 493002.

Onoda-Yamamuro, N., Matsuo, T., and Suga, H. (1990). Calorimetric and IR spectroscopic studies of phase transitions in methylammonium trihalogenoplumbates (II)†. J. Phys. Chem. Sol. 51, 1383–1395.

Pérez-Osorio, M.A., Milot, R.L., Filip, M.R., Patel, J.B., Herz, L.M., Johnston, M.B., and Giustino, F. (2015). Vibrational properties of the organic–inorganic halide perovskite $CH_3NH_3PbI_3$ from theory and experiment: factor group Analysis, first-principles calculations, and low-temperature infrared spectra. J. Phys. Chem. C 119, 25703–25718.

Poglitsch, A., and Weber, D. (1987). Dynamic disorder in methylammoniumtrihalogenoplumbates (II)

observed by millimeter-wave spectroscopy. J. Chem. Phys. 87, 6373–6378.

Quarti, C., Mosconi, E., Ball, J.M., D'Innocenzo, V., Tao, C., Pathak, S., Snaith, H.J., Petrozza, A., and De Angelis, F. (2016). Structural and optical properties of methylammonium lead iodide across the tetragonal to cubic phase transition: implications for perovskite solar cells. Energy Environ. Sci. 9, 155–163.

Quarti, C., Mosconi, E., and De Angelis, F. (2014). Interplay Orientational Order Electron. Struct. Methylammonium Lead Iodide: Implications Solar Cell Operation. Chem. Mater. 26, 6557–6569.

Ren, Y., Oswald, I.W., Wang, X., McCandless, G.T., and Chan, J.Y. (2016). Orientation of organic cations in hybrid inorganic–organic perovskite $CH_3NH_3PbI_3$ from subatomic resolution single crystal neutron diffraction structural studies. Cryst. Growth Des. 16, 2945–2951.

Röhm, H., Leonhard, T., Schulz, A.D., Wagner, S., Hoffmann, M.J., and Colsmann, A. (2019). Ferroelectric properties of perovskite thin films and their implications for solar energy conversion. Adv. Mater. 31, 1806661.

Roiland, C., Trippé-Allard, G., Jemli, K., Alonso, B., Ameline, J.-C., Gautier, R., Bataille, T., Le Polles, L., Deleporte, E., and Even, J. (2016). Multinuclear NMR as a tool for studying local order and dynamics in $CH_3NH_3PbX_3$ (X= Cl, Br, I) hybrid perovskites. Phys. Chem. Chem. Phys. 18, 27133–27142.

Rosales, B.A., Men, L., Cady, S.D., Hanrahan, M.P., Rossini, A.J., and Vela, J. (2016). Persistent dopants and phase segregation in organolead mixed-halide perovskites. Chem. Mater. 28, 6848–6859.

Rothmann, M.U., Li, W., Zhu, Y., Liu, A., Ku, Z., Bach, U., Etheridge, J., and Cheng, Y.-B. (2018). Structural and chemical changes to $CH_3NH_3PbI_3$ induced by electron and gallium ion beams. Adv. Mater 30, 1800629.

Saidaminov, M.I., Adinolfi, V., Comin, R., Abdelhady, A.L., Peng, W., Dursun, I., Yuan, M., Hoogland, S., Sargent, E.H., and Bakr, O.M. (2015). Planar-integrated single-crystalline perovskite photodetectors. Nat. Commun. 6, 1–7.

Sanchez, S., Steiner, U., and Hua, X. (2019). Phase evolution during perovskite formation—insight from pair distribution function analysis. Chem. Mater. 31, 3498–3506.

Schuck, G., Többens, D.M., Koch-Müller, M., Efthimiopoulos, I., and Schorr, S. (2018). Infrared spectroscopic study of vibrational modes across the orthorhombic–tetragonal phase transition in methylammonium lead halide single crystals. J. Phys. Chem. C 122, 5227–5237.

Selig, O., Sadhanala, A., Müller, C., Lovrincic, R., Chen, Z., Rezus, Y.L.A., Frost, J.M., Jansen, T.L.C., and Bakulin, A.A. (2017). Organic cation rotation and immobilization in pure and mixed methylammonium lead-halide perovskites. J. Am. Chem. Soc. 139, 4068–4074.

Senanayak, S.P., Yang, B., Thomas, T.H., Giesbrecht, N., Huang, W., Gann, E., Nair, B., Goedel, K., Guha, S., and Moya, X. (2017). Understanding charge transport in lead iodide

perovskite thin-film field-effect transistors. Sci. Adv. 3, e1601935.

Senocrate, A., Moudrakovski, I., Kim, G.Y., Yang, T.Y., Gregori, G., Grätzel, M., and Maier, J. (2017). The nature of ion conduction in methylammonium lead iodide: a multimethod approach. Angew. Chem. Int. Ed. 56, 7755–7759.

Seo, S., Jung, H.S., Yoo, P.J., Park, J.H., Jung, D.-Y., Shin, H., and Park, N.-G. (2019). Hot scientific debate on halide perovskites: fundamentals, photovoltaics, and optoelectronics at eighth sungkyun international solar forum 2019 (SISF 2019). ACS Energy Lett. 4, 2475–2479.

Shi, D., Adinolfi, V., Comin, R., Yuan, M., Alarousu, E., Buin, A., Chen, Y., Hoogland, S., Rothenberger, A., and Katsiev, K. (2015). Low trap-state density and long carrier diffusion in organolead trihalide perovskite single crystals. Science 347, 519–522.

Son, D.-Y., Lee, J.-W., Choi, Y.J., Jang, I.-H., Lee, S., Yoo, P.J., Shin, H., Ahn, N., Choi, M., Kim, D., et al. (2016). Self-formed grain boundary healing layer for highly efficient $CH_3NH_3PbI_3$ perovskite solar cells. Nat. Energy 1, 16081.

Stoumpos, C.C., and Kanatzidis, M.G. (2015). The renaissance of halide perovskites and their evolution as emerging semiconductors. Acc. Chem. Res. 48, 2791–2802.

Stoumpos, C.C., Malliakas, C.D., and Kanatzidis, M.G. (2013). Semiconducting tin and lead iodide perovskites with organic cations: phase transitions, high mobilities, and near-infrared photoluminescent properties. Inorg. Chem. 52, 9019–9038.

Stranks, S.D., Eperon, G.E., Grancini, G., Menelaou, C., Alcocer, M.J., Leijtens, T., Herz, L.M., Petrozza, A., and Snaith, H.J. (2013). Electron-hole diffusion lengths exceeding 1 micrometer in an organometal trihalide perovskite absorber. Science 342, 341–344.

Swainson, I., Hammond, R., Soullière, C., Knop, O., and Massa, W. (2003). Phase transitions in the perovskite methylammonium lead bromide, $CH_3ND_3PbBr_3$. J. Solid State Chem. 176, 97–104.

Tan, S., Yavuz, I., De Marco, N., Huang, T., Lee, S.-J., Choi, C.S., Wang, M., Nuryyeva, S., Wang, R., Zhao, Y., et al. (2020). Steric impediment of ion migration contributes to improved operational stability of perovskite solar cells. Adv. Mater. 32, 1906995.

Tyson, T.A., Gao, W., Chen, Y.S., Ghose, S., and Yan, Y. (2017). Large thermal motion in halide perovskites. Sci. Rep. 7, 9401.

Wang, J., Zhang, C., Liu, H., McLaughlin, R., Zhai, Y., Vardeny, S.R., Liu, X., McGill, S., Semenov, D., and Guo, H. (2019). Spin-optoelectronic devices based on hybrid organic-inorganic trihalide perovskites. Nat. Commun. 10, 1–6.

Wasylishen, R.E., Knop, O., and Macdonald, J.B. (1985). Cation rotation in methylammonium lead halides. Solid State Commun. 56, 581–582.

Weber, D. (1978). $CH_3NH_3PbX_3$, ein Pb (II)-system mit kubischer perowskitstruktur/$CH_3NH_3PbX_3$, a Pb (II)-system with cubic perovskite structure. Z. Naturforsch. B 33, 1443–1445.

Wei, J., Zhao, Y., Li, H., Li, G., Pan, J., Xu, D., Zhao, Q., and Yu, D. (2014). Hysteresis analysis based on the ferroelectric effect in hybrid perovskite solar cells. J. Phys. Chem. Lett. 5, 3937–3945.

Weller, M.T., Weber, O.J., Frost, J.M., and Walsh, A. (2015). Cubic perovskite structure of black formamidinium lead iodide, α-[HC(NH$_2$)$_2$]PbI$_3$, at 298 K. J. Phys. Chem. Lett. 6, 3209–3212.

Whitfield, P.S., Herron, N., Guise, W.E., Page, K., Cheng, Y.Q., Milas, I., and Crawford, M.K. (2016). Structures, Phase Transitions Tricritical Behav. Hybrid Perovskite Methyl Ammonium Lead Iodide. Sci. Rep 6, 35685.

Worhatch, R.J., Kim, H., Swainson, I.P., Yonkeu, A.L., and Billinge, S.J.L. (2008). Study of local structure in selected organic–inorganic perovskites in the Pm3m phase. Chem. Mater. 20, 1272–1277.

Wu, X., Tan, L.Z., Shen, X., Hu, T., Miyata, K., Trinh, M.T., Li, R., Coffee, R., Liu, S., Egger, D.A., et al. (2017). Light-induced picosecond rotational disordering of the inorganic sublattice in hybrid perovskites. Sci. Adv. 3, e1602388.

Xiao, C., Li, Z., Guthrey, H., Moseley, J., Yang, Y., Wozny, S., Moutinho, H., To, B., Berry, J.J., Gorman, B., et al. (2015). Mechanisms of electron-beam-induced damage in perovskite thin films revealed by cathodoluminescence spectroscopy. J. Phys. Chem. C 119, 26904–26911.

Xing, G., Mathews, N., Sun, S., Lim, S.S., Lam, Y.M., Grätzel, M., Mhaisalkar, S., and Sum, T.C. (2013). Long-range balanced electron-and hole-transport lengths in organic-inorganic CH$_3$NH$_3$PbI$_3$. Science 342, 344–347.

Yaffe, O., Guo, Y., Tan, L.Z., Egger, D.A., Hull, T., Stoumpos, C.C., Zheng, F., Heinz, T.F., Kronik, L., Kanatzidis, M.G., et al. (2017). Local polar fluctuations in lead halide perovskite crystals. Phys. Rev. Lett. 118, 136001.

Yang, J.M., Kim, S.G., Seo, J.Y., Cuhadar, C., Son, D.Y., Lee, D., and Park, N.G. (2018). 1D hexagonal HC(NH$_2$)$_2$PbI$_3$ for multilevel resistive switching nonvolatile memory. Adv. Electron. Mater. 4, 1800190.

Yin, W.-J., Shi, T., and Yan, Y. (2014). Unusual defect physics in CH$_3$NH$_3$PbI$_3$ perovskite solar cell absorber. Appl. Phys. Lett. 104, 063903.

Yu, Y., Zhang, D., Kisielowski, C., Dou, L., Kornienko, N., Bekenstein, Y., Wong, A.B., Alivisatos, A.P., and Yang, P. (2016). Atomic resolution imaging of halide perovskites. Nano Lett. 16, 7530–7535.

Yu, Y., Zhang, D., and Yang, P. (2017). Ruddlesden–popper phase in two-dimensional inorganic halide perovskites: a plausible model and the supporting observations. Nano Lett. 17, 5489–5494.

Zhang, D., Zhu, Y., Liu, L., Ying, X., Hsiung, C.-E., Sougrat, R., Li, K., and Han, Y. (2018). Atomic-resolution transmission electron microscopy of electron beam–sensitive crystalline materials. Science 359, 675–679.

Zhou, Y., Zhou, H., Deng, J., Cha, W., and Cai, Z. (2020). Decisive structural and functional characterization of halide perovskites with synchrotron. Matter 2, 360–377.

Zhu, F., Men, L., Guo, Y., Zhu, Q., Bhattacharjee, U., Goodwin, P.M., Petrich, J.W., Smith, E.A., and Vela, J. (2015). Shape evolution and single particle luminescence of organometal halide perovskite nanocrystals. ACS Nano 9, 2948–2959.

Zhu, H., Miyata, K., Fu, Y., Wang, J., Joshi, P.P., Niesner, D., Williams, K.W., Jin, S., and Zhu, X.-Y. (2016a). Screening in crystalline liquids protects energetic carriers in hybrid perovskites. Science 353, 1409–1413.

Zhu, Q., Zheng, K., Abdellah, M., Generalov, A., Haase, D., Carlson, S., Niu, Y., Heimdal, J., Engdahl, A., Messing, M.E., et al. (2016b). Correlating structure and electronic band-edge properties in organolead halide perovskites nanoparticles. Phys. Chem. Chem. Phys. 18, 14933–14940.